Tetrahedron 69 (2013) 712–721

Contents lists available at SciVerse ScienceDirect

Tetrahedron

journal homepage: www.elsevier.com/locate/tet

Synthesis, structural analysis and application of a series of solid-state fluorochromes—aryl hydrazones of 4-hydrazino-*N*-hexyl-1,8-naphthalimide

Ivaylo P. Ivanov [a,*], Mashenka B. Dimitrova [b], Donka N. Tasheva [c], Diana V. Cheshmedzhieva [c], Valentin S. Lozanov [d], Sonia V. Ilieva [c]

[a] Faculty of Biology, Sofia University, 1164 Sofia, Bulgaria
[b] Institute of Experimental Morphology, Pathology and Anthropology with Museum, Bulgarian Academy of Sciences, 1113 Sofia, Bulgaria
[c] Faculty of Chemistry and Pharmacy, Sofia University, 1164 Sofia, Bulgaria
[d] Department of Medical Chemistry and Biochemistry, Medical University of Sofia, 1431 Sofia, Bulgaria

ARTICLE INFO

Article history:
Received 14 June 2012
Received in revised form 12 October 2012
Accepted 29 October 2012
Available online 10 November 2012

Keywords:
1,8-Naphthalimide
Hydrazone
Chemical shift
Hammett correlation
Mass spectrometry
Solid-state fluorescence
Enzyme activity imaging

ABSTRACT

The development of red solid-state fluorochromes is important for different applications. The influence of the electronic effects of substituents on the chemical shifts in the ^{1}H NMR spectra and solid-state fluorescent properties of aryl hydrazones of 4-hydrazino-*N*-hexyl-1,8-naphthalimide is evaluated. The main fragmentation pathway of hydrazones is determined using electrospray ionization mass spectrometry and high resolution MS/MS. A possible application of these fluorochromes for the in situ imaging of enzyme activities is presented.

© 2012 Elsevier Ltd. All rights reserved.

1. Introduction

1,8-Naphthalimides have been widely studied due to their photophysical properties. These are one of the most important building blocks for the synthesis of efficient fluorescent materials showing strong fluorescence, large quantum yields and sizable Stokes shifts. Naphthalimides are widely used as colourants in the polymer industry,[1,2] laser dyes,[1,3,4] chemosensors[5,6] and fluorescence probes for biomedical purposes, including fluorescence cell makers[7] and anti-cancer agents.[8] Efficient solid-state emission of organic materials is essential for optoelectronic devices, and the molecular design and development of novel fluorochromes that emit visible light in the solid state with high efficiency are strongly desired for different applications.[9] Though many organic compounds show red fluorescence in solution, fewer compounds fluoresce in the solid state due to intermolecular interactions in the condensed states.[10] Gan and co-workers[11,12] have synthesized several aryl hydrazones of 4-hydrazino-*N*-butyl-1,8-naphthalimide and studied their electronic and fluorescence spectra for application as materials for organic light-emitting diodes (OLEDs). The authors have mentioned that materials for green and blue OLEDs are available, whereas red fluorescent materials of high efficiency are not common. Photophysical properties of the other synthesized hydrazones of 1,8-naphthalimide have been investigated,[13,14] including those covalently bound to single-wall carbon nanotubes[15] and components of copolymers.[16–18] Naphthalimide hydrazones based on vanillin[19] and salicylaldehyde[20] were designed and synthesized as highly selective fluorescent probes for Ag^+ and Cu^{2+}, respectively.

Correlation analysis, the study of the relationships between the parameters known as substituent constants and various directly measurable quantities, plays an important role in physical organic chemistry for the description of the electronic properties of molecules. Free energy relationships have been observed for a number of spectroscopic properties,[21] including mass spectrometry.[21,22] Correlation analyses have also been applied to demonstrate that dependencies exist between substituent effect and chemical shifts in nuclear magnetic resonance spectroscopy.[23,24] So, the established relationships are of substantial value for the prediction of NMR properties.[25]

* Corresponding author. Tel.: +359 2 8167 214; e-mail address: ivayloi@abv.bg (I.P. Ivanov).

0040-4020/$ – see front matter © 2012 Elsevier Ltd. All rights reserved.
http://dx.doi.org/10.1016/j.tet.2012.10.093

Fluorescence-based imaging of enzyme activity in vitro and in vivo promises many applications from elucidation of the enzyme function and mechanism, to better disease detection and monitoring.[26–28] The possibility for application of 1,8-naphthalimide hydrazones for fluorescent histochemical localization of enzymes—markers for malignant or other diseases has been explored. Members of our group have developed methods for fluorescent histochemical localization of dipeptidyl peptidase IV, tripeptidyl peptidase I[29] and gamma-glutamyl transpeptidase.[30] The enzyme hydrolyzes the corresponding synthetic substrate to yield free 4-hydrazino-*N*-hexyl-1,8-naphthalimide, which couples simultaneously with piperonal and gives a water-insoluble fluorescent hydrazone precipitating on the sites of enzyme activity and marking them.

In the present work, a series of substituted aryl hydrazones of 4-hydrazino-*N*-hexyl-1,8-naphthalimide were synthesized and characterized by nuclear magnetic resonance and mass spectrometry. The effects of substituents at the benzene ring on the ^{1}H NMR chemical shifts have been studied using models, based on mono and dual substituent parameter relationship. Electrospray ionization mass spectrometry (ESI-MS) and high resolution MS/MS have been used in order to explore the general and specific fragmentation of the compounds studied. The substituent effect on the solid-state fluorescence properties has been rationalized using Hammett type correlation, and the possibilities for application of the series of hydrazones to develop new techniques for fluorescent imaging of enzyme activity have been explored.

2. Results and discussion

2.1. Synthesis

The most common method for the preparation of *N*-substituted hydrazones is the reaction of aldehydes or ketones with *N*-alkyl or *N*-aryl hydrazines.[31] Usually the reaction proceeds in ethanol solution under reflux for a few hours. *N*-Aryl hydrazones and especially those substituted with electron-withdrawing groups are stable to acids and can be prepared under acidic conditions. In a previous work[29] we described the synthesis of the piperonal hydrazone of 4-hydrazino-*N*-hexyl-1,8-naphthalimide in the presence of acetic acid. In the present study this approach is successfully applied for the preparation of a series of substituted aryl hydrazones of *N*-hexyl-1,8-naphthalimide (Scheme 1).

2.2. Effect of phenyl substituents on the proton chemical shift

According to the principle of substituent-induced changes in the chemical shift (SCS), the variations in the ^{1}H NMR spectra of hydrazones **3a**–**3g** were correlated using different linear free energy relationship (LFER) models, based on the mono and dual substituent parameters (σ_p, σ_p^+, *F*, *R* and R^+). The protons chemical shifts (δ_H), which correlate with the Hammett type substituent constants are shown in Table 1. Good linear correlation (n=7, r=0.9865) between the chemical shift of the amine hydrogen (N*H*) and σ_p substituent constants was observed for this series (Fig. 1). The slope ρ is 0.34±0.02. A similar dependence (ρ=0.65±0.03) was observed in the series of *N*-phenylhydrazones of *p*-substituted benzaldehydes.[32] In these compounds the sensitivity to the electronic effects of substituents is double that of the established for *N*-hexyl-1,8-naphthalimide hydrazones (**3a**–**3g**).

Table 1
NMR chemical shifts (δ_H) for two types of hydrogen atoms in the series of *p*-substituted hydrazones **3a**–**3g** and Hammett substituent constants correlating with the respective chemical shifts

Compound		δ_H[a] (ppm)		Hammett substituent constants[b]		
	X	N*H*	H-5	σ_p	σ_p^+	*R*
3a	$N(CH_3)_2$	11.25	7.65	−0.83	−1.70	−0.98
3b	OCH_3	11.39	7.70	−0.27	−0.78	−0.56
3c	CH_3	11.46	7.74	−0.17	−0.31	−0.18
3d	H	11.52	7.77	0.00	0.00	0.00
3e	Cl	11.54	7.73	0.23	0.11	−0.19
3f	CN	11.72	7.78	0.66	0.66	0.15
3g	NO_2	11.82	7.84	0.78	0.79	0.13

[a] Solvent—CD_3SOCD_3.
[b] Taken from Ref. 33.

The observed LFER in the two series of hydrazones shows that shielding/deshielding of the N*H* hydrogen atoms is determined from the nitrogen atom shielding/deshielding caused by the electronic effect of the aromatic ring substituents. The excellent linear correlation (r=0.9957) obtained between δ_H and M06/6-31+G(d) computed Hirshfeld charges on the amine nitrogen for *N*-methyl analogues of **3a**–**3g**[14] also supports this assumption (Fig. S1 in the Supplementary data).

Hammett correlations of ^{15}N NMR chemical shifts of the amine and imine type nitrogen atoms (δ_N) with σ_p constants in the series of *N*-phenyl[34] and *N*-alkyl-*N*-(2-hydroxycyclohexyl)[35] hydrazones of *p*-substituted benzaldehydes have also been determined. In both cases ρ is negative. This indicates that electron-withdrawing (EW) substituents cause deshielding of the nitrogen atoms, whereas electron-donating (ED) substituents cause shielding effects. The resonance structure **4** has the main contribution[34–36] to the electron density distribution in hydrazones (Scheme 2). Electron-withdrawing substituents increase the stability of this structure[35,37,38] by field and resonance (form **5**) effects. In contrast, ED substituents increase the stability of resonance forms **6** and **7** (Scheme 2). To estimate the influence of the field and resonance

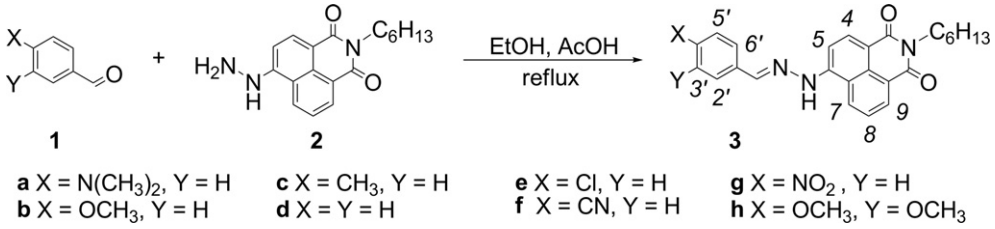

Scheme 1. Synthesis of hydrazones **3a**–**h**.

The reactions between aldehydes **1a**–**1h** and 4-hydrazino-1,8-naphthalimide (**2**) were carried out under reflux in ethanol solution in the presence of acetic acid for several minutes. The reaction time depends on the electronic effects of the substituents. The reaction between *p*-nitrobenzaldehyde and **2** was carried out for 5 min, whereas the interaction with *p*-dimethylaminobenzaldehyde was completed in 15 min. Hydrazones **3b**–**3h** precipitated on cooling; compound **3g** crystallized partially during the reaction. For the isolation of hydrazone **3a** a few drops of water were added to the solution and the resulting solid was filtered. The crude crystalline compounds were purified by column chromatography.

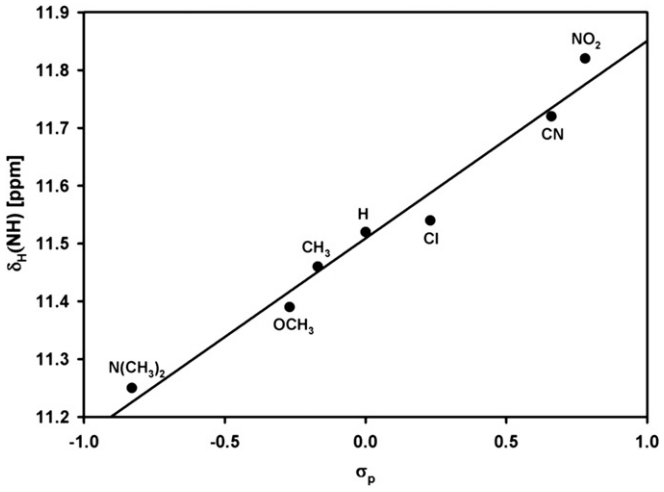

Fig. 1. Plot of the N*H* hydrogen NMR chemical shifts for the series of *p*-substituted hydrazones **3a**–**3g** in CD_3SOCD_3 versus Hammett substituent constants σ_p.

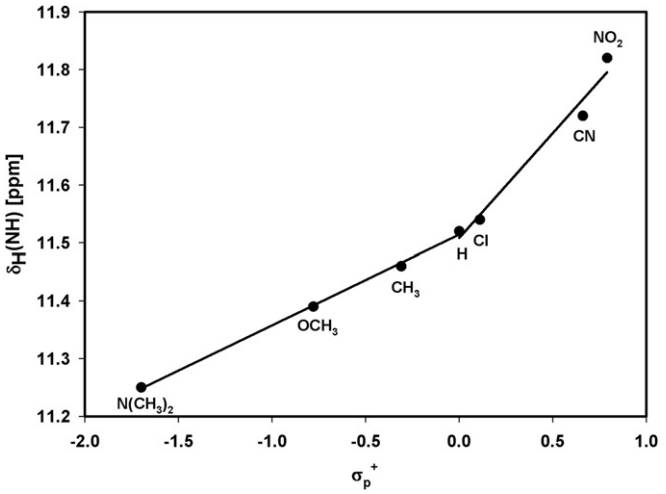

Fig. 2. Plot of the N*H* hydrogen NMR chemical shifts for the series of *p*-substituted hydrazones **3a**–**3g** in CD_3SOCD_3 versus Hammett substituent constants σ_p^+.

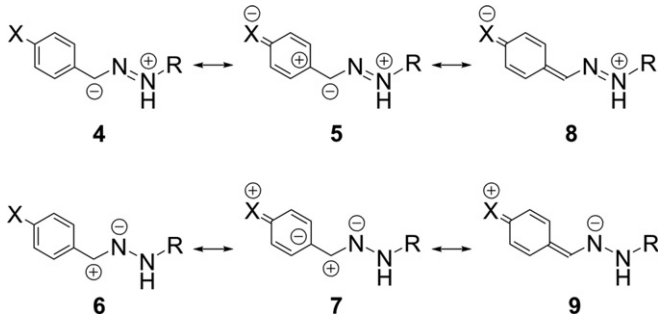

Scheme 2. Resonance structures of *p*-substituted hydrazones **3a**–**3g** involving *p*-substituents and the benzylidene hydrazine moiety.

effects on δ_H(N*H*) a model based on the dual substituent parameter (Swain–Lupton type equation) has been used for regression analysis in the following form (Eq. 1):

$$SCS = \rho_F F + \rho_R R + h \quad (1)$$

In Eq. 1 *F* and *R* are substituent parameters reflecting the field and resonance electronic effects, respectively, ρ_F and ρ_R indicate the sensitivity of the chemical shift to the field and resonance electronic effects of the aromatic ring substituents. Good correlation (n=7, r=0.987) in the series **3a**–**3g** was observed; the parameters ρ_F=0.33±0.07 and ρ_R=0.35±0.04 were obtained. Therefore, the influence of the field and resonance electronic effects are equal and the contribution of the resonance forms **4** and **5** is equivalent. The same is valid also for the resonance forms **6** and **7**.

Neuvonen et al.[35] studied the electronic structures of a series of imines and hydrazones by ^{13}C and ^{15}N NMR spectroscopy. The authors carried out statistical analysis of the Hammett type correlations and established fair linear correlation between chemical shifts of the amine type hydrogen and σ_p^+ constants of the substituents. However, the Hammett plot (δ_H(N*H*) versus σ_p^+(X)) for substituent X variations in the series of *N*-hexyl-1,8-naphthalimide hydrazones (**3a**–**3g**) is in fact biphasic concave upwards (Fig. 2) with a break at σ_p^+=0.00 (X=H). The point of the unsubstituted compound and the points of the hydrazones with ED substituents are on a line with ρ_{ED}=0.157±0.005 (n=4, r=0.9991). The second segment of the plot, which includes EW substituents is steeper (ρ_{EW}=0.36±0.04; n=3, r=0.9872). We established that the plot of Hirshfeld charges of the amine nitrogen atom of **3a**–**3g** versus σ_p^+ substituent constants was also biphasic concave upwards with a break at σ_p^+=0.00 (Fig. S2 in Supplementary data). The dependence from σ_p^+ constants is an indicator for a direct conjugation between the substituent and the nitrogen atom in the hydrazones. EW substituents stabilize[34] the resonance form **8**, whereas ED substituents stabilize[38] the resonance form **9** (Scheme 2). By using a dual substituent parameter model (Eq. 1) for the first segment of Fig. 2, where *R* substituent parameters are replaced by R^+ parameters, the following values were obtained: ρ_F=0.146±0.048 and ρ_R^+=0.156±0.008 (n=4, r=0.999). These results indicate that the resonance forms **6** and **9** have equal contribution to the molecular electron density distribution. The polar effects of EW substituents are larger and practically identical (ρ_F=0.36±0.10 and ρ_R^+=0.38±0.13; n=3, r=0.982) and the contributions of the resonance forms **4** and **8** are also identical. In 1-(4-nitrobenzylidene)-2-phenylhydrazine the resonance structure[29] **8** has a significant contribution. The absorption spectra of *N*-hexyl-1,8-naphthalimide hydrazones with EW substituents in acetonitrile showed a hypsochromic shift.[14] However, the nitro-substituted compound **3g** showed a bathochromic shift of 13 nm. This effect might be due to the formation of a quinone type structure with a significant contribution to the resonance structure **8**. The resonance stabilization **4**↔**5**↔**8** allows free rotation around the C=N bond and leads to the rapid conversion between isomeric forms.[37] This free rotation could explain the fact that in the ^1H NMR spectrum of **3g** the signals are broad and without expressed multiplicity unlike the other hydrazones in the series.

To determine whether the formation of biphasic Hammett correlation is typical for hydrazones, the data for δ_N of the amine nitrogen atoms in *N*-phenyl-[34] and *N*-alkyl-(2-hydroxycyclohexyl)[35] hydrazones of *p*-substituted benzaldehydes were used. The correlations for both series are also biphasic concave upwards with a break at σ_p^+=0.00 (Fig. S3 in Supplementary data). The comparison of the Hammett type correlations in different series of hydrazones shows that the electron effects of the two types of substituents are typical for this class of compounds.

The amine nitrogen lone pair conjugates with the naphthalimide moiety leading to the formation of resonance structure **10** and **11** (Scheme 3). It conjugates also with the other part of the molecule (Scheme 2) thus connecting the benzylideneamino and naphthalimide moieties. The presence of such conjugation is demonstrated by using the LFER model (Fig. 3), where the excellent correlation between δ_H(H-5) and *R* substituent constants with ρ=0.115±0.007 (n=6, r=0.9923) is observed. This effect could be explained by the resonance form **12** (Scheme 3), in which the

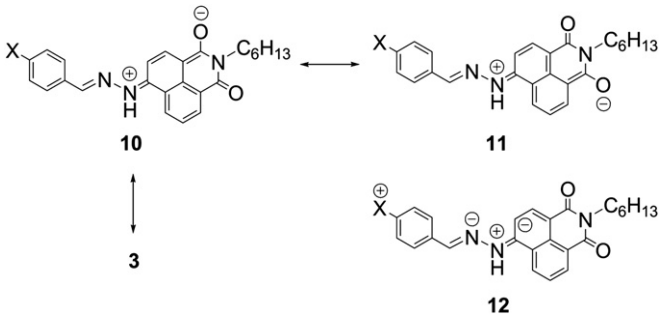

Scheme 3. Resonance structures for the series of *p*-substituted hydrazones **3a**–**3g** involving benzylidene hydrazine and naphthalimide moieties.

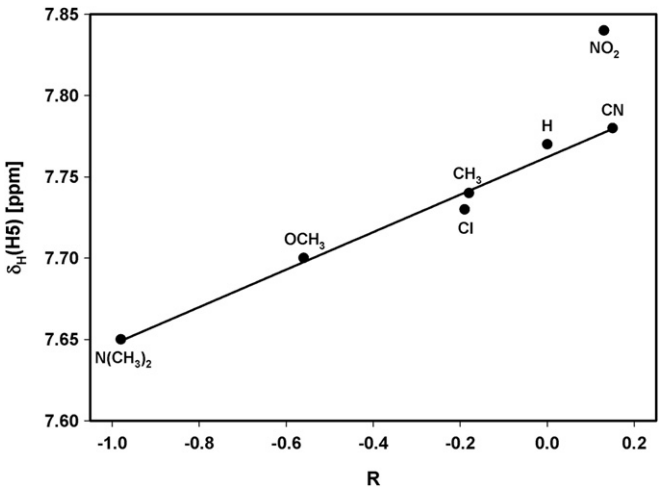

Fig. 3. Hammett type plot of the H-5 hydrogen atom NMR chemical shifts for the series of *p*-substituted hydrazones **3a**–**3g** in CD_3SOCD_3 versus *R* substituent constants. Compound **3g** (X=NO_2) is outside of the established trend for the series studied.

substituents with +*R*-effect stabilize the structure, while substituents with −*R*-effect destabilize it. The hydrazone **3g** (X=NO_2) is outside of the established trend for the series studied, probably due to the large contribution of the resonance structure **8** for this compound.

In a previous work we performed a full geometry optimization for *N*-methyl analogues of hydrazones **3a**–**3g** in acetonitrile by using PCM computations.[14] According to these results ED substituents shorten the C1′–C(H) bond length thus making the N–N bond longer as a result of the stabilization by resonance structure **9** and make the resonance stabilization **6**↔**7**↔**9** favourable (Scheme 2). The considerable contribution of the resonance form **9** is supported by the bathochromic effect caused by ED substituents in the absorption spectra of hydrazones in acetonitrile.[14] EW substituents make the C=N longer and the bond N–N shorter in compliance with the increased contribution of the resonance stabilization **4**↔**5**↔**8**. The ED and EW kinds of substituents have opposite effects on the N–C6 bond length. ED substituents make this bond shorter by the stabilization effect **11**↔**12** (Scheme 3), while EW substituents make it longer by destabilizing these resonance forms.

2.3. Electrospray ionization mass spectrometry

Hydrazones are important derivatives for structural and quantitative characterization of carbonyl compounds, including carbohydrates, in environmental analysis, food chemistry and industrial analysis by chromatography, fluorescence spectroscopy, and mass spectrometry.[39,40] The detailed cognition of the fragmentation behaviour of hydrazones is an additional demonstration for their structure and is significant to the analytical practice.[41,42]

Electrospray ionization (ESI) in positive and negative mode was used for the structure elucidation of the investigated compounds **3a**–**3h**, as the hydrazones form stable protonated $[M+H]^+$ or deprotonated $[M-H]^-$ ions. High resolution MS/MS experiments in the positive mode proved to be more informative to study these compounds due to the formation of more ions during the fragmentation of $[M+H]^+$. The mass spectrum of unsubstituted hydrazone **3d** is presented in Fig. 4 and the characteristic ions for this series of hydrazones are given in Table 2. The main fragmentation pathway of compounds **3a**–**3h** is presented in Scheme 4. The proposed fragmentation patterns are supported by high resolution mass spectrometry (HRMS). The proposed structure of the ions is given in Fig. S4 in the Supplementary data.

LC–ESI-MS/MS experiments showed that the fragmentation of $[M+H]^+$ ions involves loss of 1-hexene leading to $[MH-C_6H_{12}]^+$ ions with a high relative intensity (Scheme 4; route a). The formation of these ions takes place throughout McLafferty rearrangement. There is a dependence between the electronic effect of substituents and the relative intensity of these ions. Hydrazones with strong ED substituents (**3a**, **3b** and **3h**) have a relative intensity of 100%, whereas for those with EW substituents the intensity is below 50% (Table 2). The $[MH-C_6H_{12}]^+$ ions give rise to ions of moderate intensity with *m*/*z* 212 (Table 2). Accurate mass measurement of the ion *m*/*z* 212 in the mass spectrum of **3d** is 212.0587. The measured mass of this ion in the other hydrazones is practically the same. However, *m*/*z* 212.0587 does not give the correct composition of the ion with relative error less than 10 ppm. The unsubstituted hydrazone **3d** contains naphthalene and cyclic imide moieties. The fragmentation of naphthalene and its derivatives is characterized by a loss of acetylene.[43,44] On the other hand, the aromatic cyclic imides,[45] including naphthalimides[46] lose CO to give fragment ions. Ions with *m*/*z* 212 can be formed in two ways (Scheme 4; route a_1 and a_2). Through the route a_1, acetylene and the related benzene are lost corresponding to 212(I) ion with the theoretical mass of *m*/*z* 212.0454. According to the route a_2, after the loss of CO and the corresponding cyclohexa-1,3-dien-5-yne, an ion 212(II) with theoretical mass of *m*/*z* 212.0818 should be formed. In our experimental conditions, even at high resolutions, these two ions could not be resolved. These ions are formed also from the *m*/*z* 296 ion, which is the most intense in the mass spectra of the hydrazones (Table 2). In compounds **3c**–**3g** *m*/*z* 296 shows a relative intensity of 100%, whereas in the hydrazones with substituents with strong ED properties this intensity is between 58% and 86%. However, the analysis of the results showed that it is composed of two unresolved ions: 296(I) (theoretical mass 296.1393; route b) and 296(II) (theoretical mass 296.1757; route c). The *m*/*z* 296(I) is formed by a cleavage of the bond between the imine carbon atom and the benzene ring[47] accompanied by a loss of acetylene. The *m*/*z* 296(II) ion is formed by cleavage of the same bond but CO is lost instead of acetylene in this case. The loss of 1-hexene from these two ions (296(I) and 296(II)) leads to the formation of ions 212(I) and 212(II) correspondingly. An ion with *m*/*z* 279 of low intensity (Scheme 4, route d) is observed in the mass spectra of hydrazones. It is formed throughout a loss of neutral fragments in the route c accompanied by elimination of NH_3. After the loss of the respective phenylmethanimine from the molecular ion (route f) an ion with *m*/*z* 295 is formed. Its relative intensity varied from moderate (**3b**) to very low (**3f** and **3g**). Except for **3a**, the fragmentation of $[M+H]^+$ ions by the loss of corresponding benzonitrile (route e) after the cleavage of N–N bond,[47] leads to the formation of the *m*/*z* 297 ion of low or very low intensity (Table 2). The elimination of 1-hexene from this ion leads to the protonated form of 4-amino-1,8-naphthalimide with *m*/*z* 213 (Scheme 4). The intensity of *m*/*z* 213 depends on the electronic effect of substituent: it varies from moderate for ED substituents to very low for EW substituents.

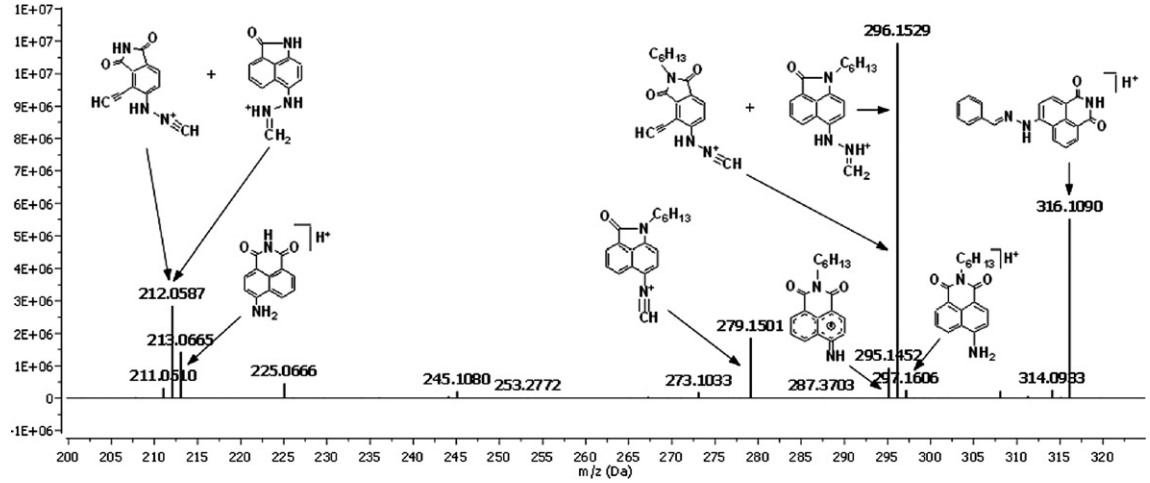

Fig. 4. High resolution ESI(+) mass spectrum of the unsubstituted hydrazone **3d**.

Table 2
Selected general fragments in the ESI(+) mass spectra of hydrazones **3a**–**3h** and their relative intensity. Elemental composition could be assigned to experimental *m*/*z* values with relative errors below 10 ppm

Ion	Compound (X/Y)							
Calcd *m*/*z*	**3a**	**3b**	**3c**	**3d**	**3e**	**3f**	**3g**	**3h**
Elemental	$N(CH_3)_2$	OCH_3	CH_3	H	Cl	CN	NO_2	OCH_3
Composition	H	H	H	H	H	H	H	OCH_3
	Accurate *m*/*z* determination (relative error [ppm]; relative intensity [%])							
M-83[a]	359.1515	346.1182	330.1239	316.1090	350.0689	341.1039	361.0937	376.1290
	(3.6; 100)	(1.1; 100)	(0.7; 80)	(2.9; 50)	(0.5; 44)	(1.7; 27)	(1.6; 31)	(0.4; 100)
	Calcd 359.1502	Calcd 346.1186	Calcd 330.1237	Calcd 316.1080	Calcd 350.0691	Calcd 341.1033	Calcd 361.0931	Calcd 376.1292
297.1597	297.1601	297.1590	297.1571	297.1606	297.1587	297.1608	297.1585	297.1597
$C_{18}H_{21}N_2O_2$	(1.1; 82)	(2.6; 8)	(8.9; 11)	(3.0; 4)	(3.4; 2)	(3.7; 1)	(4.2; 11)	(0.1; 8)
296.1757	296.1519	296.1516	296.1520	296.1529	296.1516	296.1524	296.1524	296.1519
(II) $C_{18}H_{22}N_3O$	(80; 58)	(81; 86)	(80; 100)	(77; 100)	(81; 100)	(79: 100)	(79; 100)	(80; 70)
296.1393	296.1519	296.1516	296.1520	296.1529	296.1516	296.1524	296.1524	296.1519
(I) $C_{17}H_{18}N_3O_2$	(42; 58)	(41; 86)	(43; 100)	(46; 100)	(41; 100)	(44: 100)	(44; 100)	(42; 70)
295.1441	295.1450	295.1439	295.1445	295.1452	295.1441	295.1444	295.1447	295.1444
$C_{18}H_{19}N_2O_2$	(3.2; 11)	(0.6; 26)	(1.3; 16)	(3.6; 8)	(0.1; 10)	(1.0; 1)	(2.2; 1)	(0.9; 17)
279.1492	279.1500	279.1491	279.1494	279.1501	279.1481	279.1497	279.1496	279.1493
$C_{18}H_{19}N_2O$	(2.9; 13)	(0.3; 13)	(1.0; 12)	(3.2; 17)	(3.9; 13)	(1.9; 8)	(1.6; 11)	(0.4; 12)
213.0658	213.0664	213.0656	213.0660	213.0665	213.0663	213.0662	213.0645	213.0659
$C_{12}H_9N_2O_2$	(2.7; 27)	(1.2; 27)	(0.7; 17)	(3.0; 13)	(2.2; 9)	(1.7; 1)	(6.2; 1)	(0.1; 20)
212.0818	212.0586	212.0579	212.0583	212.0587	212.0574	212.0584	212.0582	212.0580
(II) $C_{12}H_{10}N_3O$	(109; 11)	(113; 18)	(111; 16)	(109; 26)	(115; 18)	(110; 10)	(111; 17)	(112; 19)
212.0454	212.0586	212.0579	212.0583	212.0587	212.0574	212.0584	212.0582	212.0580
(I) $C_{11}H_6N_3O_2$	(62; 11)	(58; 18)	(60; 16)	(63; 26)	(57; 18)	(61; 10)	(60; 17)	(59; 19)

[a] *m*/*z* of ions $[MH-C_6H_{12}]^+$.

Several characteristic ions are observed in the mass spectra of hydrazones with ED substituents **3a**, **3b** and **3h** (Scheme S1 in Supplementary data). In these three compounds an ion with *m*/*z* 322 is detected. Its intensity is high for **3a** and low for **3b** and **3h**. This ion is obtained from $[M+H]^+$ ions through the loss of the corresponding substituted benzene. The following elimination of 1-hexene leads to an *m*/*z* 238 ion. For **3a** and **3h**, ions of low intensity are registered. They are formed after a loss of NH_3 or HCN from $[M+H]^+$ ions. In the mass spectrum of **3a** ($X=N(CH_3)_2$) a specific ion with *m*/*z* 398 and middle intensity is observed. It is formed by elimination of dimethylamine. A specific ion (*m*/*z* 333) for **3h** ($X=Y=OCH_3$) results after the loss of CO, HCN and pentane.

2.4. Solid-state fluorescence properties

Previously, we synthesized the hydrazone of 4-hydrazino-*N*-hexyl-1,8-naphthalimide with piperonal (**3i**).[29] Its solid-state fluorescence was excited by violet and green light. The fluorescent properties of the crystals were studied for all hydrazones. Using violet light, the fluorescence is yellow-green and red, whereas green light leads to a red fluorescence (Fig. S5). According to Gan et al.[12] the fluorescence of the hydrazone of 4-hydrazino-*N*-butyl-1,8-naphthalimide with *p*-dimethylaminobenzaldehyde is rosy in colour and of low intensity. We observed a highly intensive red fluorescence of the dimethylamino substituted hydrazone (**3a**). On the other hand, the *p*-nitro substituted compound **3g** does not fluoresce.

Next, we studied the effect of the substituents on the solid-state (crystals) fluorescence properties at λ_{ex}=390 nm. The normalized fluorescence spectra for the entire series of compounds are shown in Fig. 5. The spectral shapes of substituted aryl hydrazones of *N*-hexyl-1,8-naphthalimide are similar to each other. In the spectral band a long wavelength shoulder is observed, which is only hinted at in the cases of **3d** and **3e**. The emission band of **3a** ($X=N(CH_3)_2$) is situated in the red light area (Fig. 5). That is why the fluorescence colour is red only. The emission maxima (F_{max}) and full width at the

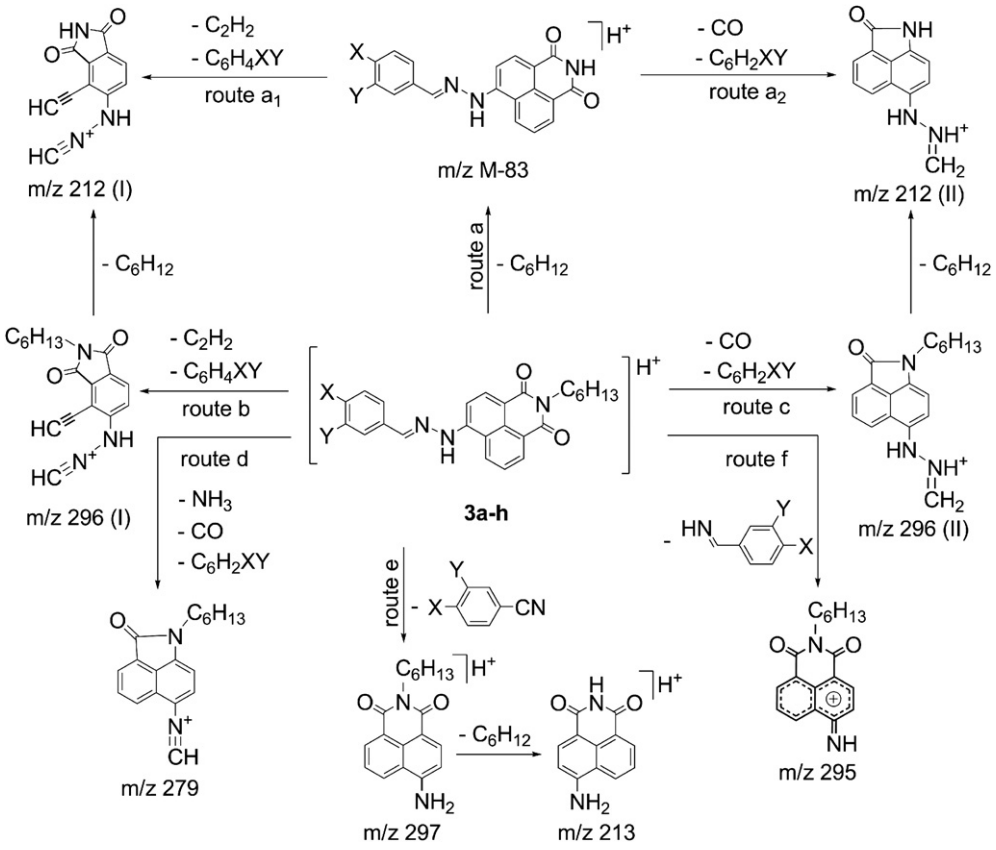

Scheme 4. The main fragmentation pathway of hydrazones **3a**–**3h** under ESI(+) MS conditions.

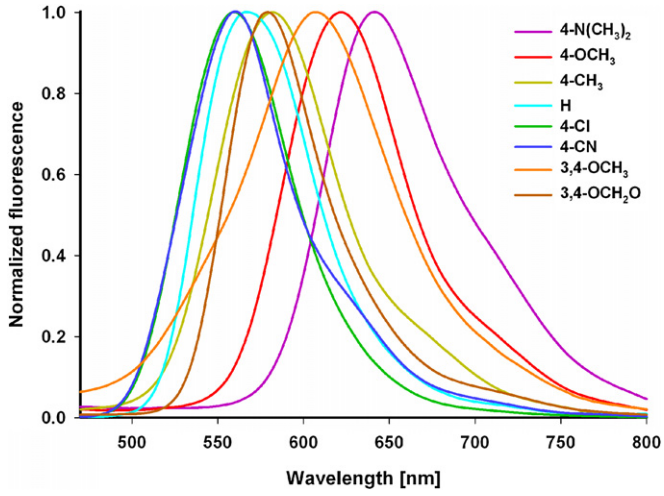

Fig. 5. Normalized emission spectra (λ_{ex}=390 nm) of hydrazones **3a**–**3f**, **3h** and **3i** in solid-state (crystals).

half maxima (FWHM) are presented in Table 3. The electron accepting cyano group causes a small (7 nm) hypsochromic shift in F_{max}. The ED substituents generally lead to large bathochromic shifts of the emission maxima, especially in the cases of **3b** (F_{max}=622 nm) and **3a** (F_{max}=643 nm) compared to F_{max}=567 nm for the unsubstituted compound (Table 3). The experimental emission wavelengths for *p*-substituted hydrazones correlate excellently with R^+ constants with ρ=−43±3 (n=5, r=0.9915), compound **3e** (X=Cl) being out of the trend (Fig. 6). An intramolecular

Table 3
The emission maxima (F_{max}) and full width at the half maxima of hydrazones **3a**–**3f**, **3h** and **3i** in solid-state (λ_{ex}=390 nm)

	Compound		F_{max} (nm)	ΔF[a] (nm)	FWHM (nm)
	X	Y			
3a	$N(CH_3)_2$	H	643	73	90
3b	OCH_3	H	622	76	82
3c	CH_3	H	582	49	80
3d	H	H	567	41	76
3e	Cl	H	562	39	74
3f	CN	H	560	48	73
3h	OCH_3	OCH_3	608	59	103
3i[b]	OCH_2O		580	33	61

[a] ΔF=F_{max}(solid)−F_{max}(acetonitrile solution).
[b] The hydrazone **3i** was synthesized as described in Ref. 29.

charge transfer takes place from the aryl moiety towards the naphthalimide part of the molecule in the hydrazones excited state.[14] In the solid state, this transition is facilitated by the substituents with +*R*-effect, whereas their inductive effect does not influence F_{max}.

The solid-state fluorescence spectra of the crystalline forms are red-shifted by 33–76 nm compared to those in solution (Table 3) indicating the presence of intermolecular interactions in the solid state. The red-shift (ΔF, Table 3) for the substituted hydrazones is larger than ΔF of the unsubstituted compound (**3d**), except for **3e** (X=Cl) and **3i** (X=Y=OCH_2O). This shift increases with the enhancement of the +*R*-effect of the substituent. The lower red shift (ΔF) of *p*-chloro derivative leading to a decline from the Hammett type correlation is most probably due to the particular type of its crystal structure. Most probably the stacking interactions in the solid state prevent the intramolecular charge transfer.

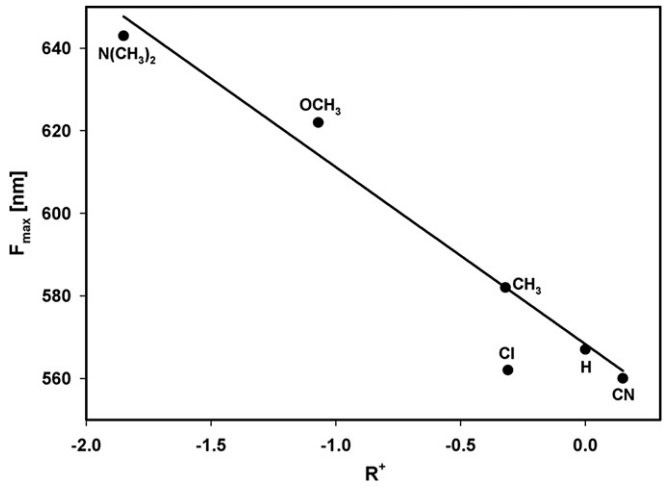

Fig. 6. Dependence between experimental emission maxima and R^+ Hammett constants for the series of *p*-substituted hydrazones **3a**–**3f**. Compound **3e** (X=Cl) is outside of the trend established for this series.

The full width at the half maximum depends on the electronic effect of substituents. It varies from 61 nm for **3i** to 103 nm for **3h** (X=Y=OCH_3). The spectral band of **3h** covers the area from 420 to 800 nm (Fig. 5). For the series of *p*-substituted hydrazones a Hammett type correlation (n=6, r=0.9823) is determined between FWHM and σ_p^+ constants of substituent X (Fig. 7). The slope is negative (ρ=−7.4±0.7) to show that EW substituents shorten the full width at the half maximum, whereas ED substituents lengthen it (Table 3).

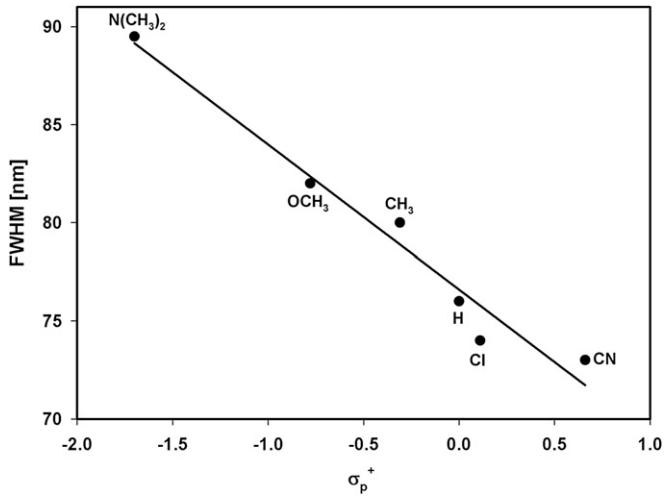

Fig. 7. Linear correlation of the full width at the half maxima for the series of *p*-substituted hydrazones **3a**–**3f** against σ_p^+ Hammett parameters.

2.5. Enzyme activity imaging

The synthesized 1,8-naphthalimide hydrazones can be used for the fluorescent in situ imaging of enzyme activities according to the previously described principle.[29] Briefly, the enzyme substrates represent amino acid or peptide hydrazides of 4-hydrazino-*N*-hexyl-1,8-naphthalimide. The enzyme cleaves the hydrazide bond and the released hydrazine reacts simultaneously with an aromatic aldehyde to give a water-insoluble hydrazone precipitating on the enzyme sites and marking them by an intensive fluorescence. As it was described above, the emission maxima and full width at the half maxima of hydrazones in the solid state depend on the electronic effect of the benzene ring substituents. Thus, a fluorescent enzyme imaging of different fluorescence colour and intensity can be achieved by varying the aldehyde used as a visualization agent. Usually, fluorochromes with emission maxima in the red area of the visible spectrum are preferred due to the lack of background noise caused by tissues autofluorescence.[48]

We tested different aldehydes for the localization of dipeptidyl peptidase IV (DPPIV) and gamma-glutamyl transpeptidase (GGT) activities in cryosections of rat organs according to the above principle. Examples of the enzymes activities imaging are given in Fig. 8. Best results were obtained with **1a**, **1b**, **1e**, **1f** and **1h**. Using all these aldehydes, precise enzyme activity localization was observed. The specificity of the enzyme reactions was confirmed by inhibition studies using irreversible inhibitors. The fluorescent signal in the preparations was strong and stable upon excitation (Fig. 8b, d). At the same time, the red colour of the corresponding hydrazones permits observations by light microscopy as well (Fig. 8a, c). The histochemical samples are stable and can be studied several weeks after the preparation.

3. Conclusions

Eight substituted aryl hydrazones of 4-hydrazino-*N*-hexyl-1,8-naphthalimide were synthesized. A linear correlation between chemical shift of the hydrogen, bonded to the amine type nitrogen atom (N*H*) and σ_p constants of the substituents was observed for the series of *p*-substituted hydrazones (**3a**–**3g**). The influence of both field and resonance electronic effects and the contribution of different resonance forms were evaluated using a model based on the dual substituent parameters. The Hammett type correlation between δ_H(N*H*) and σ_p^+ constants of the substituents was biphasic concave upwards with a break at σ_p^+=0.00 (X=H). The excellent correlation between δ_H(H-5) from naphthalimide moiety and R substituent constants was observed to show that the amine nitrogen puts together the two parts (benzylideneamino and naphthalimide) in the hydrazone molecule in the ground state. The main fragmentation pathway of hydrazones **3a**–**3h** was determined using electrospray ionization mass spectrometry and high resolution MS/MS. The highest relative intensity in the mass spectra of the compounds was observed for $[MH-C_6H_{12}]^+$ ions and the ions with m/z 296. The solid-state fluorescence of all the hydrazones was yellow-green and red, except for the *p*-nitro substituted compound, which did not fluoresce. It was shown that a correlation exists between experimental emission maxima and R^+ Hammett constants for the series of *p*-substituted hydrazones **3a**–**3f** (compound **3e** (X=Cl) is outside of the trend). A linear correlation of full width at the half maxima of these hydrazones against σ_p^+ Hammett parameters was observed. It was shown that the newly developed histochemical method based on the formation of fluorescent hydrazones as final reaction products is suitable for the in situ imaging of the enzyme activity. The proposed histochemical method allows a precise localization of the enzymes since the red emission eliminates the fluorescent background noise. The fluorescence in the preparations is stable upon excitation and histochemical samples can be used at least for several weeks.

The synthesized hydrazones have the useful quality of stable red colour fluorescence in solid state. The study presented here allows predicting their fluorescent properties depending on the electronic effect of substituents in order to choose the most appropriate compound for any particular application.

4. Experimental section

4.1. General

^{1}H NMR spectra were obtained using a Bruker Avance AV II+600 MHz NMR spectrometer and tetramethyl silane as an internal standard in CD_3SOCD_3 as a solvent. Chemical shifts (δ) are

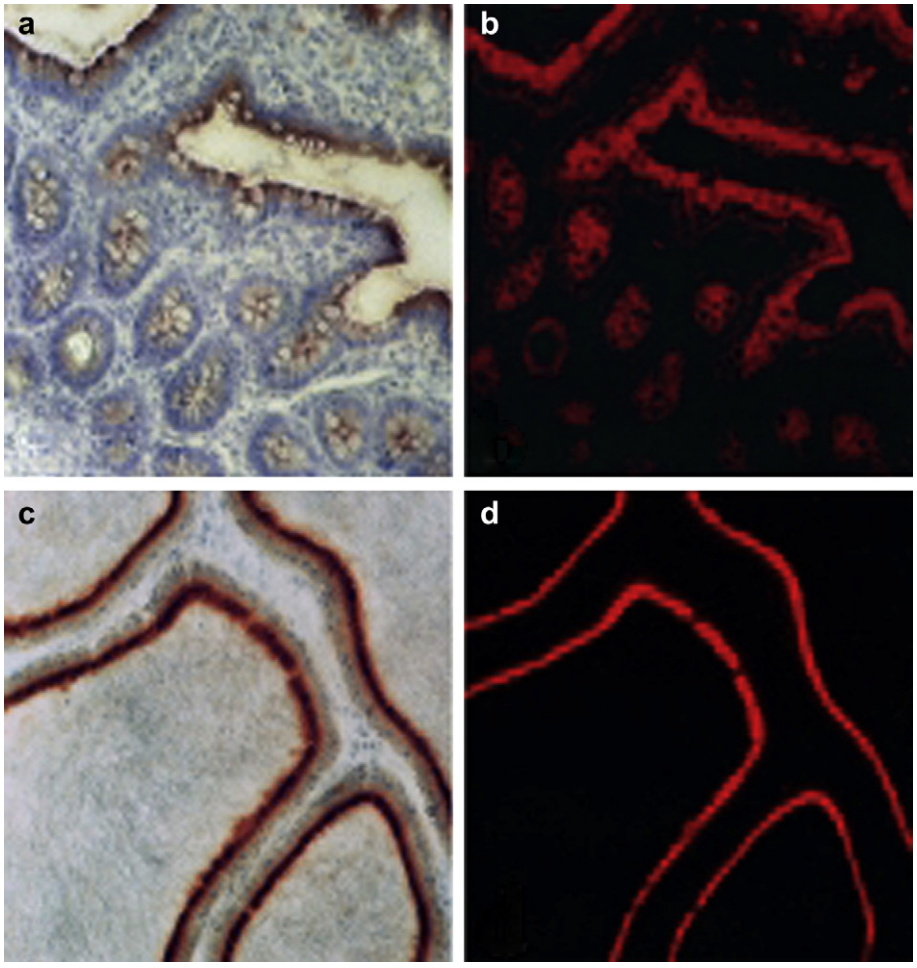

Fig. 8. Fluorescent imaging of enzymes in the cryosections of rat organs using substrates based on 4-hydrazino-*N*-hexyl-1,8-naphthalimide and different aldehydes as visualization agents. DPPIV activity localized by the substrate 4-Gly-Pro-hydrazido-*N*-hexyl-1,8-naphthalimide and 4-dimethylaminobenzaldehyde (a, b)—the enzyme is active in the brush border area of small intestinal enterocytes. GGT activity visualized by γ-Glu-hydrazido-*N*-hexyl-1,8-naphthalimide and 4-chlorobenzaldehyde (c, d)—the enzyme activity is restricted to the stereocilia of epithelial cells of the epididymis channels. Light microscopy (a, c); fluorescent microscopy (b, d). Original magnifications 200×.

expressed in parts per million and coupling constants (*J*) in hertz. Multiplicity and qualifier abbreviations are as follows: s=singlet, d=doublet, dd=doublet of doublet, t=triplet, br s=broad singlet and m=multiplet.

IR spectra were scanned on FTIR (Shimadzu IRPrestige-21) in Nujol.

The chromatographic separation of the compounds was carried out on an Surveyor® Plus HPLC system, which consisted of a binary gradient pump, autosampler and PDA detector (ThermoScientific Co, USA) by X-Bridge C_{18} column (I.D. 2.1 mm×150 mm, particle size 3.5 μm, Waters Corporation, USA) using as eluents: A—0.1% formic acid in water; B—0.1% formic acid in acetonitrile at flow rate of 250 μL/min. The following binary gradient was used: 60–100% B for 10 min; 100% B for 5 min and 100–60% B for 3 min.

Mass spectrometric investigations were performed on LTQ Orbitrap® Discovery mass spectrometer (ThetmoScientific Co, USA) equipped with electrospray ionization module IonMax® (ThetmoScientific Co, USA).

Full-scan spectra over the *m*/*z* range 200–1000 were acquired in the positive and negative ion modes. The Orbitrap® was operated at resolution settings of 30,000. All the Orbitrap® MS parameters were optimized using the instrument control software program. The following parameters were used: spray voltage 3.8 kV, spray current 100 μA, sheath gas flow rate 30 AU, auxiliary gas flow rate 0, sweep gas flow rate 5 AU, capillary voltage 10 V, capillary temperature 300 °C and tube lens voltage 70 V.

MS/MS experiments were carried out in the positive mode of operation using normalized collision dissociation (CID) energy values of 30% AU for all of the compounds. The fragment ions were detected in Orbitrap® analyzer at 15,000 preselected resolution.

Data acquisition and processing were carried out with XCalibur® software package (ThetmoScientific Co, USA).

Measurements of fluorescence spectra were performed on Varian Cary Eclipse (λ_{ex}=390 nm).

Elemental analyses were performed by VarioEL V5, CHNS Mode, Elementar Analysensysteme GmbH. Microanalyses (C, H, N) of new compounds were in agreement with the theoretical values within ±0.3%. Melting points were determined on a Botius micro melting point apparatus and were uncorrected.

Tissue sections were cut on cryotome Reichert-Jung, model 2800 (Germany). Enzyme reactions were observed under microscope OPTON IM 35 (Germany).

The 4-hydrazino-*N*-butyl-1,8-naphthalimide was synthesized as described before.[29] The DPPIV inhibitor (*N*-(Phe-Pro)-*O*-(4-nitrobenzoyl)hydroxylamine hydrochloride) was synthesized after Demuth et al.[49] The GGT inhibitor 6-diazo-5-oxo-norleucine and all the organic solvents and aldehydes were purchased from Sigma–Aldrich (Germany). Acetonitrile LC–MS Chromasolv®, formic acid eluent additive for LC–MS and silica gel 60 (0.063–0.200 mm) for column chromatography were from Fluka (Germany). Aluminium oxide 90 neutral (0.063–0.250 mm) for column chromatography was from Merck (Germany).

4.2. Synthesis of hydrazones

A mixture of **2** (0.062 g, 0.2 mmol) and the corresponding benzaldehyde (0.2 mmol) in ethanol (2.8 mL) was refluxed for 5–15 min in the presence of acetic acid (10 μL). The solution was allowed to crystallize at room temperature. The obtained precipitate was filtered, washed with cold ethanol and purified by recrystallisation (**3a**) or column chromatography on silica gel (**3b**–**3f**, **3h**) or aluminium oxide (**3g**).

*4.2.1. 6-(2-(4-(Dimethylamino)benzylidene)hydrazinyl)-2-hexyl-1H-benzo[de]isoquinoline-1,3(2H)-dione (**3a**).* To the cold solution, water (250 μL) was added. The obtained precipitate was filtered and recrystallized from ethanol/water to yield compound **3a** (0.048 g, 54%) as dark purple crystals; mp 215–217 °C; ^{1}H NMR δ (ppm): 11.25 (s, 1H, N*H*N═), 8.78 (d, *J*=8.4 Hz, 1H, H-9), 8.47 (d, *J*=7.2 Hz, 1H, H-7), 8.35 (s, 1H, C*H*═N), 8.35 (d, *J*=8.9 Hz, 1H, H-4), 7.76 (dd, *J*=8.0, 7.6 Hz, 1H, H-8), 7.65 (d, *J*=8.5 Hz, 1H, H-5), 7.63 (d, *J*=8.8 Hz, 2H, H-2′, H-6′), 6.79 (d, *J*=8.8 Hz, 2H, H-3′, H-5′), 4.04–3.99 (m, 2H, NCH_2), 3.00 (s, 6H, –N(CH_3)$_2$), 1.65–1.57 (m, 2H, NCH$_2$CH_2), 1.37–1.25 (m, 6H, CH$_2$CH$_2$(CH_2)$_3$), 0.87 (t, *J*=6.9 Hz, 3H, CH_3). Selected IR data ν (cm^{-1}): 3308 (NH), 1685 (C═O), 1635 (C═N), 1616 (C═N); HRMS calcd for $C_{27}H_{31}N_4O_2$ [M+H]$^+$ *m*/*z* 443.2441, found HRMS-ESI(+) *m*/*z* 443.2445. Anal. Calcd for $C_{27}H_{30}N_4O_2$: C, 73.28; H, 6.83; N, 12.66%, found: C, 73.01; H, 6.65; N, 12.77%.

*4.2.2. 2-Hexyl-6-(2-(4-methoxybenzylidene)hydrazinyl)-1H-benzo[de]isoquinoline-1,3(2H)-dione (**3b**).* The crude product was chromatographed (dichloromethane/hexane/isopropanol, 1:3:0.1) to yield compound **3b** (0.038 g, 44%) as red crystals; mp 195–197 °C; ^{1}H NMR δ (ppm): 11.39 (s, 1H, N*H*N═), 8.79 (d, *J*=8.4 Hz, 1H, H-9), 8.48 (d, *J*=7.3 Hz, 1H, H-7), 8.42 (s, 1H, C*H*═N), 8.42 (d, *J*=8.5 Hz, 1H, H-4), 7.79 (dd, *J*=8.2, 7.4 Hz, 1H, H-8), 7.76 (d, *J*=8.7 Hz, 2H, H-2′, H-6′), 7.70 (d, *J*=8.5 Hz, 1H, H-5), 7.05 (d, *J*=8.8 Hz, 2H, H-3′, H-5′), 4.04–3.99 (m, 2H, NCH_2), 3.83 (s, 3H, CH_3OC$_6$H$_4$), 1.65–1.57 (m, 2H, NCH$_2$CH_2), 1.37–1.25 (m, 6H, CH$_2$CH$_2$(CH_2)$_3$), 0.87 (t, *J*=7.0 Hz, 3H, CH_3). Selected IR data ν (cm^{-1}): 3315 (NH), 1683 (C═O), 1641 (C═O), 1616 (C═N), 1251 (C–O–C), 1029 (C–O–C); HRMS calcd for $C_{26}H_{28}N_3O_3$ [M+H]$^+$ *m*/*z* 430.2125, found HRMS-ESI(+) *m*/*z* 430.2126. Anal. Calcd for $C_{26}H_{27}N_3O_3$: C, 72.71; H, 6.34; N, 9.78%, found: C, 72.94; H, 6.25; N, 9.62%.

*4.2.3. 2-Hexyl-6-(2-(4-methylbenzylidene)hydrazinyl)-1H-benzo[de]isoquinoline-1,3(2H)-dione (**3c**).* The crude product was chromatographed (dichloromethane/hexane/isopropanol, 1:3:0.1) to yield compound **3c** (0.037 g, 45%) as orange crystals; mp 185–187 °C; ^{1}H NMR δ (ppm): 11.46 (s, 1H, N*H*N═), 8.81 (dd, *J*=8.5, 0.8 Hz, 1H, H-9), 8.49 (dd, *J*=7.2, 0.9 Hz, 1H, H-7), 8.44 (s, 1H, C*H*═N), 8.38 (d, *J*=8.5 Hz, 1H, H-4), 7.80 (dd, *J*=8.4, 7.3 Hz, 1H, H-8), 7.74 (d, *J*=8.5 Hz, 1H, H-5), 7.72 (d, *J*=8.1 Hz, 2H, H-2′, H-6′), 7.30 (d, *J*=7.9 Hz, 2H, H-3′, H-5′), 4.05–3.98 (m, 2H, NCH_2), 2.37 (s, 3H, CH_3C$_6$H$_4$), 1.66–1.58 (m, 2H, NCH$_2$CH_2), 1.37–1.26 (m, 6H, CH$_2$CH$_2$(CH_2)$_3$), 0.87 (t, *J*=7.0 Hz, 3H, CH_3). Selected IR data ν (cm^{-1}): 3291 (NH), 1691 (C═O), 1635 (C═O), 1616 (C═N); HRMS calcd for $C_{26}H_{28}N_3O_2$ [M+H]$^+$ *m*/*z* 414.2176, found HRMS-ESI(+) *m*/*z* 414.2173. Anal. Calcd for $C_{26}H_{27}N_3O_2$: C, 75.52; H, 6.58; N, 10.16%, found: C, 75.38; H, 6.44; N, 10.05%.

*4.2.4. 6-(2-Benzylidenehydrazinyl)-2-hexyl-1H-benzo[de]isoquinoline-1,3(2H)-dione (**3d**).* The crude product was chromatographed (dichloromethane/hexane/isopropanol, 1:6:0.1) to yield compound **3d** (0.027 g, 34%) as yellow crystals. Yield 0.027 g (34%), crystals; mp 207–209 °C; ^{1}H NMR δ (ppm): 11.52 (s, 1H, N*H*N═), 8.82 (d, *J*=8.4 Hz, 1H, H-9), 8.50 (d, *J*=7.2 Hz, 1H, H-7), 8.48 (s, 1H, C*H*═N), 8.40 (d, *J*=8.5 Hz, 1H, H-4), 7.83 (d, *J*=7.2 Hz, 2H, H-2′, H-6′), 7.82 (dd, *J*=8.0, 7.3 Hz, 1H, H-8), 7.77 (d, *J*=8.5 Hz, 1H, H-5), 7.50 (t, *J*=7.4 Hz, 2H, H-3′, H-5′), 7.44 (t, *J*=7.3 Hz, 1H, H-4′), 4.05–4.00 (m, 2H, NCH_2), 1.65–1.58 (m, 2H, NCH$_2$CH_2), 1.37–1.27 (m, 6H, CH$_2$CH$_2$(CH_2)$_3$), 0.87 (t, *J*=7.0 Hz, 3H, CH_3). Selected IR data ν (cm^{-1}): 3283 (NH), 1685 (C═O), 1632 (C═O), 1616 (C═N); HRMS calcd for $C_{25}H_{26}N_3O_2$ [M+H]$^+$ *m*/*z* 400.2019, found HRMS-ESI(+) *m*/*z* 400.2021. Anal. Calcd for $C_{25}H_{25}N_3O_2$: C, 75.16; H, 6.31; N, 10.52%, found: C, 74.96; H, 6.59; N, 10.37%.

*4.2.5. 6-(2-(4-Chlorobenzylidene)hydrazinyl)-2-hexyl-1H-benzo[de]isoquinoline-1,3(2H)-dione (**3e**).* The crude product was chromatographed (dichloromethane/hexane/isopropanol, 1:5:0.1) to yield compound **3e** (0.050 g, 58%) as yellow crystals; mp 188–190 °C; ^{1}H NMR δ (ppm): 11.54 (s, 1H, N*H*N═), 8.78 (d, *J*=8.4 Hz, 1H, H-9), 8.47 (d, *J*=7.2 Hz, 1H, H-7), 8.42 (s, 1H, C*H*═N), 8.36 (d, *J*=8.5 Hz, 1H, H-4), 7.83 (d, *J*=8.5 Hz, 2H, H-2′, H-6′), 7.81–7.77 (m, 1H, H-8), 7.73 (d, *J*=8.5 Hz, 1H, H-5), 7.53 (d, *J*=8.4 Hz, 2H, H-3′, H-5′), 4.02–3.98 (m, 2H, NCH_2), 1.64–1.56 (m, 2H, NCH$_2$CH_2), 1.31 (dt, *J*=14.0, 7.3 Hz, 6H, CH$_2$CH$_2$(CH_2)$_3$), 0.86 (t, *J*=6.9 Hz, 3H, CH_3). Selected IR data ν (cm^{-1}): 3309 (NH), 1695 (C═O), 1638 (C═O), 1616 (C═N), 1093 (C-Cl); HRMS calcd for $C_{25}H_{25}ClN_3O_2$ [M+H]$^+$ *m*/*z* 434.1630 and 436.1600, found HRMS-ESI(+) *m*/*z* 434.1631 and 436.1595 (30%). Anal. Calcd for $C_{25}H_{24}ClN_3O_2$: C, 69.20; H, 5.57; N, 9.68%, found: C, 69.23; H, 5.77; N, 9.56%.

*4.2.6. 4-((2-(2-Hexyl-1,3-dioxo-2,3-dihydro-1H-benzo[de]isoquinolin-6-yl)hydrazono)methyl)benzonitrile (**3f**).* The crude product was chromatographed (dichloromethane/hexane/isopropanol, 1:3:0.1) to yield compound **3f** (0.036 g, 42%) as yellow crystals; mp 175–177 °C; ^{1}H NMR δ (ppm): 11.72 (s, 1H, N*H*N═), 8.79 (d, *J*=8.5 Hz, 1H, H-9), 8.48 (d, *J*=7.2 Hz, 1H, H-7), 8.45 (s, 1H, C*H*═N), 8.38 (d, *J*=8.4 Hz, 1H, H-4), 7.97 (d, *J*=8.1 Hz, 2H, H-2′, H-6′), 7.91 (d, *J*=8.1 Hz, 2H, H-3′, H-5′), 7.81 (t, *J*=7.8 Hz, 1H, H-8), 7.78 (d, *J*=8.4 Hz, 1H, H-5), 4.00 (t, *J*=7.5 Hz, 2H, NCH_2), 1.64–1.57 (m, 2H, NCH$_2$CH_2), 1.36–1.25 (m, 6H, CH$_2$CH$_2$(CH_2)$_3$), 0.87 (t, *J*=6.5 Hz, 3H, CH_3). Selected IR data ν (Nujol, cm^{-1}): 3307 (NH), 2228 (C≡N), 1691 (C═O), 1638 (C═O), 1616 (C═N); HRMS calcd for $C_{26}H_{25}N_4O_2$ [M+H]$^+$ *m*/*z* 425.1972, found HRMS-ESI(+) *m*/*z* 425.1973. Anal. Calcd for $C_{26}H_{24}N_4O_2$: C, 73.56; H, 5.70; N, 13.20%, found: C, 73.37; H, 5.64; N, 12.98%.

*4.2.7. 2-Hexyl-6-(2-(4-nitrobenzylidene)hydrazinyl)-1H-benzo[de]isoquinoline-1,3(2H)-dione (**3g**).* The crude product was chromatographed on neutral aluminium oxide (dichloromethane/hexane/isopropanol, 1:5:0.1) to yield compound **3g** (0.045 g, 51%) as orange-red crystals; mp 231–233 °C; ^{1}H NMR δ (ppm): 11.82 (s, 1H, NH), 8.88–8.77 (m, 1H, H9), 8.58–8.46 (m, 2H, H7 & CH═N), 8.41 (br s, 1H, H4), 8.35–8.26 (m, 2H, H3′ & H5′), 8.11–8.01 (m, 2H, H2′ & H6′), 7.90–7.79 (m, 2H, H5 & H8), 4.09–3.95 (m, 2H, NCH$_2$), 1.72–1.52 (m, 2H, NCH$_2$CH_2), 1.39–1.14 (m, 6H, NCH$_2$(CH_2)$_3$), 0.93–0.81 (m, 3H, CH$_3$). Selected IR data ν (cm^{-1}): 3313 (NH), 1690 (C═O), 1644 (C═O), 1616 (C═N), 1512 (NO$_2$), 1337 (NO$_2$); HRMS calcd for $C_{25}H_{25}N_4O_4$ [M+H]$^+$ *m*/*z* 445.1870, found HR-ESI(+) *m*/*z* 445.1864. Anal. Calcd for $C_{25}H_{24}N_4O_4$: C, 67.55; H, 5.44; N, 12.60%, found: C, 67.35; H, 5.30; N, 12.78%.

*4.2.8. 6-(2-(3,4-Dimethoxybenzylidene)hydrazinyl)-2-hexyl-1H-benzo[de]isoquinoline-1,3(2H)-dione (**3h**).* The crude product was chromatographed (dichloromethane/hexane/isopropanol, 1:6:0.1) to yield compound **3h** (0.039 g, 42%) as red crystals; mp 148–150 °C; ^{1}H NMR δ (ppm): 11.39 (s, 1H, N*H*N═), 8.79 (d, *J*=8.5 Hz, 1H, H-9), 8.48 (dd, *J*=7.3, 1.0 Hz, 1H, H-7), 8.39 (s, 1H, C*H*═N), 8.37 (d, *J*=8.5 Hz, 1H, H-4), 7.79 (dd, *J*=8.4, 7.3 Hz, 1H, H-8), 7.74 (d, *J*=8.5 Hz, 1H, H-5), 7.45 (d, *J*=1.9 Hz, 1H, H-2′), 7.27 (dd, *J*=8.4, 1.9 Hz, 1H, H-6′), 7.05 (d, *J*=8.4 Hz, 1H, H-5′), 4.03–3.99 (m, 2H, NCH_2), 3.89 (s, 3H, CH_3OC$_6$H$_4$), 3.83 (s, 3H, CH_3OC$_6$H$_4$), 1.65–1.57 (m, 2H, NCH_2), 1.36–1.28 (m, 6H) CH$_2$CH$_2$(CH_2)$_3$, 0.87 (t, *J*=7.1 Hz,

3H, CH_3). Selected IR data ν (cm^{-1}): 3302 (NH), 1685 (C=O), 1639 (C=O), 1616 (C=N), 1269 (C–O–C), 1022 (C–O–C); HRMS calcd for $C_{27}H_{30}N_3O_4$ $[M+H]^+$ m/z 460.2231, found HR-ESI(+) m/z 460.2232. Anal. Calcd for $C_{27}H_{29}N_3O_4$: C, 70.57; H, 6.36; N, 9.14%, found: C, 70.40; H, 6.51; N, 8.94%.

4.3. Enzyme histochemistry

Mature male Wistar rats were decapitated under deep anaesthesia. Pieces of the small intestine and epididymis were extracted and immediately frozen in liquid nitrogen. Tissue sections (10 μm) were cut at −25 °C and mounted on gelatinized glass slides. All the sections were covered by 1% celloidine in acetone/diethyl ether/ethanol 4:3:3 for a minute at room temperature.

For the imaging of DPPIV the sections were incubated in a substrate medium consisting of 0.5 mM substrate (4-Gly-Pro-hydrazido-*N*-hexyl-1,8-naphthalimide) and 0.5 mg/mL aromatic aldehyde in 0.1 M phosphate buffer, pH 7.8 for an hour at 37 °C.

For the imaging of GGT activity the sections were incubated in a substrate solution, consisting of 0.5 mM substrate (γ-Glu-hydrazido-*N*-hexyl-1,8-naphthalimide), 0.5 mg/mL aromatic aldehyde and 5 mM glycyl-glycine in 0.1 M phosphate buffer, pH 8.2 for 3–4 h at 37 °C.

After the incubation all the sections were post-fixed in 4% neutral formalin for 15 min at room temperature, stained with haematoxyline consistent with classical methods of histology and embedded in glycerol/jelly.

Control sections for DPPIV were pre-incubated in 0.5 mM solution of the inhibitor (*N*-(Phe-Pro)-*O*-(4-nitrobenzoyl)hydroxylamine hydrochloride) in 0.1 M phosphate buffer, pH 7.8 for an hour at room temperature. After that, the sections were moved to full substrate medium, supplied with 0.5 mM inhibitor and incubated for 60 min at 37 °C. Afterwards they were treated as above.

Control sections for GGT were pre-incubated in 0.2 mM solution of the inhibitor 6-diazo-5-oxo-norleucine in 0.1 M acetate buffer, pH 7.0 for 40 min at room temperature. After that, they were moved to full substrate media, supplied with 0.2 mM inhibitor and incubated for 3 h at 37 °C. Afterwards they were treated as above.

Acknowledgements

This research was supported by FP7-REGPOT-2011-1 project Beyond Everest and the University of Sofia grant 55/2010.

Supplementary data

Supplementary data associated with this article can be found in the online version, at http://dx.doi.org/10.1016/j.tet.2012.10.093. These data include MOL files and InChiKeys of the most important compounds described in this article.

References and notes

1. McGehee, M. D.; Heeger, A. J. *Adv. Mater.* **2000**, *12*, 1655.
2. Bojinov, V.; Grabchev, I. *Dyes Pigments* **2001**, *51*, 57.
3. Tian, H.; He, Y.; Chang, C. P. *J. Mater. Chem.* **2000**, *10*, 2049.
4. Yang, S.; Meng, F.; Tian, H.; Chen, K. *Eur. Polym. J.* **2002**, *38*, 911.
5. Duke, R. M.; Veale, E. B.; Pfeffer, F. M.; Kruger, P. E.; Gunnlaugsson, T. *Chem. Soc. Rev.* **2010**, *39*, 3936.
6. Parkesh, R.; Veale, E. B.; Gunnlaugsson, T. In *Chemosensors: Principles, Strategies, and Applications*; Wang, B., Anslyn, E. V., Eds.; John Wiley & Sons: 2011; p 229.
7. Qian, X.; Xiao, Y.; Xu, Y.; Guo, X.; Qian, J.; Zhu, W. *Chem. Commun.* **2010**, 6418.
8. Braña, M. F.; Ramos, A. *Curr. Med. Chem. Anti-cancer Agents* **2001**, *1*, 237.
9. Shimizu, M.; Hiyama, T. *Chem. Asian J.* **2010**, *5*, 1516.
10. Matsui, M.; Ikeda, R.; Kubota, Y.; Funabiki, K. *Tetrahedron Lett.* **2009**, *50*, 5047.
11. Gan, J.; Tian, H.; Wang, Z.; Chen, K.; Hill, J.; Lane, P. A.; Rahn, M. D.; Fox, A. M.; Bradley, D. D. C. *J. Organomet. Chem.* **2002**, *645*, 168.
12. Gan, J.-A.; Song, Q. L.; Hou, X. Y.; Chen, K.; Tian, H. *J. Photochem. Photobiol., A* **2004**, *162*, 399.
13. Gudeika, D.; Lygaitis, R.; Mimaite, V.; Grazulevicius, J. V.; Jankauskas, V.; Lapkowski, M.; Data, P. *Dyes Pigments* **2011**, *91*, 13.
14. Cheshmedzhieva, D.; Ivanova, P.; Stoyanov, S.; Tasheva, D.; Dimitrova, M.; Ivanov, I.; Ilieva, S. *Phys. Chem. Chem. Phys.* **2011**, *13*, 18530.
15. Zhu, W.; Minami, N.; Kazaoui, S.; Kim, Y. *J. Mater. Chem.* **2004**, *14*, 1924.
16. Jin, Z. N.; Xu, Q. F.; Lu, J. M.; Yan, F.; Xia, X. W.; Wang, L. H.; Li, N. J. *Chin. Sci. Bull.* **2009**, *54*, 59.
17. Jin, Z. N.; Li, N. J.; Lu, J. M.; Xu, Q. F.; Xia, X. W.; Ge, J. F.; Wang, L. H. *E-Polymers* **2010**, No. 060.
18. Li, H.; Li, N.; Sun, R.; Gu, H.; Ge, J.; Lu, J.; Xu, Q.; Xia, X.; Wang, L. *J. Phys. Chem.* **2011**, *115*, 8288.
19. Zhou, Y.; Zhou, H.; Ma, T.; Zhang, J.; Niu, J. *Spectrochim. Acta, Part A* **2012**, *88*, 56.
20. Yang, H.; Song, H.; Zhu, Y.; Yang, S. *Tetrahedron Lett.* **2012**, *53*, 2026.
21. Topsom, R. D. In *Progress in Physical Organic Chemistry*; Taft, R. W., Ed.; John Wiley & Sons: 1987; Vol. 16, p 193.
22. Howe, I. In *Mass Spectrometry (Specialist Periodical Reports)*; Williams, D. H., Ed.; Chemical Society: 1973; Vol. 2, p 33.
23. Tribble, M. T.; Traynham, J. G. In *Advances in Linear Free Energy Relationships*; Chapman, N. B., Shorter, J., Eds.; Plenum: 1972; p 143.
24. Ewing, D. F. In *Correlation Analysis in Chemistry. Recent Advances*; Chapman, N. B., Shorter, J., Eds.; Plenum: 1978; p 357.
25. Abraham, R. J.; Mobli, M. In *Modelling ^{1}H NMR Spectra of Organic Compounds. Theory, Applications and NMR Prediction Software*; John Wiley and Sons: 2008; p 67.
26. Baruch, A.; Jeffery, D. A.; Bogyo, M. *Trends Cell Biol.* **2004**, *14*, 29.
27. Van Noorden, C. J. F. *J. Histochem. Cytochem.* **2010**, *58*, 481.
28. Razgulin, A.; Ma, N.; Rao, J. *Chem. Soc. Rev.* **2011**, *40*, 4186.
29. Ivanov, I.; Tasheva, D.; Todorova, R.; Dimitrova, M. *Eur. J. Med. Chem.* **2009**, *44*, 384.
30. Dimitrova, M.; Tasheva, D.; Ivanov, I. *Compt. Rend. Acad. Bulg. Sci.* **2011**, *64*, 1701.
31. Clark, J. S. In *Comprehensive Organic Functional Group Transformations I*; Katritzky, A. R., Meth-Cohn, O., Rees, C. W., Eds.; Elsevier: 1995; Vol. 3, p 443.
32. Buzykin, B. I.; Titova, Z. S.; Cherepinskii-Malov, V. D.; Gazetdinova, N. G.; Stolyarov, A. P.; Litvinov, I. A.; Struchkov, Yu. T.; Kitaev, Yu. P. *Russ. Chem. Bull.* **1983**, *32*, 485.
33. Hansch, C.; Leo, A.; Taft, R. W. *Chem. Rev.* **1991**, *91*, 165.
34. Westerman, P. W.; Botto, R. E.; Roberts, J. D. *J. Org. Chem.* **1978**, *43*, 2590.
35. Neuvonen, K.; Fülöp, F.; Neuvonen, H.; Koch, A.; Kleinpeter, E.; Pihlaja, K. *J. Org. Chem.* **2003**, *68*, 2151.
36. Lu, S. I. *J. Comput. Chem.* **2011**, *32*, 730.
37. Gordon, M. S.; Sojka, S. A.; Krause, J. G. *J. Org. Chem.* **1984**, *49*, 97.
38. Neuvonen, H.; Fülöp, F.; Neuvonen, K.; Koch, A.; Kleinpeter, E. J. *Phys. Org. Chem.* **2008**, *21*, 173.
39. Vogel, M.; Buldt, A.; Karst, U. *Fresenius' J. Anal. Chem.* **2000**, *366*, 781.
40. Morelle, W.; Michalski, J.-C. *Curr. Anal. Chem.* **2005**, *1*, 29.
41. Berdyshev, E. V. *Biochim. Biophys. Acta* **2011**, *1811*, 680.
42. Lattova, E.; Snovida, S.; Perreault, H.; Krokhin, O. *J. Am. Soc. Mass Spectrom.* **2005**, *16*, 683.
43. Granucci, G.; Ellinger, Y.; Boissel, P. *Chem. Phys.* **1995**, *191*, 165.
44. Van Der Hart, W. J. *Int. J. Mass Spectrom.* **2002**, *214*, 269.
45. Blanco, M. M.; Salerno, A.; Perillo, I. A. *Arkivoc* **2010**, 215.
46. Krotz, L.; Seraglia, R.; Traldi, P.; Guidugli, F.; Kavka, J.; Gaozza, C. *Org. Mass Spectrom.* **1991**, *26*, 862.
47. Seleem, H. S.; El-Inany, G. A.; El-Shetary, B. A.; Mousa, M. A.; Hanafy, F. I. *Chem. Cent. J.* **2011**, *5* Art. no. 20.
48. Raap, A. K. *Histochemistry* **1986**, *84*, 317.
49. Demuth, H. U.; Baumgrass, R.; Schaper, C.; Fischer, G.; Barth, A. *J. Enzyme Inhib.* **1988**, *2*, 129.